WELDING RESEARCH

SUPPLEMENT TO THE *WELDING JOURNAL*, JULY 1992

Sponsored by the American Welding Society and the Welding Research Council

Weldability and Hot Ductility of Chromium-Modified Ni_3Al Alloys

The influence of chromium content and heat treatment on hot cracking susceptibility is defined

BY M. C. MAGUIRE, G. R. EDWARDS AND S. A. DAVID

ABSTRACT. Hot ductility and weldability of four chromium-modified Ni_3Al alloys were characterized. The chromium content in the alloys varied from 2 to 8 at.-%, and two heat treatments were used to change the ordered microstructure: an anneal at 1190°C (2174°F) with a furnace cool, or an anneal at 1240°C (2264°F) or 1270°C (2318°F) followed by an oil quench. Different annealing temperatures and variation in cooling rates produced significantly different microstructures in the alloys. Oil quenching produced fine antiphase domains (APD) in the higher chromium alloys; whereas, no such substructure was prevalent in slowly cooled microstructures of the same alloy.

Hot ductility tests conducted on heating showed that higher chromium alloys were more ductile in the oil-quenched condition. For example, at 600°C (1274°F) an 8 at.-% chromium alloy in the oil-quenched condition exhibited 16% reduction in area; whereas, in the furnace-cooled condition, ductility fell to 9%. Chromium additions also increased the flow and fracture stress. The fracture stress increased from 700 MPa (102 ksi) in a 2 at.-% chromium alloy to 1200 MPa (174 ksi) in an 8 at.-% alloy.

These results correlated well with cracking response during autogenous electron beam (EB) welding. Full penetration EB welds were made at speeds of 2.1 to 25.4 mm/s (5 to 60 in./min) on each alloy. HAZ cracking tendency decreased with higher chromium additions, and it was completely eliminated in the 8 at.-% chromium alloy. The improved hot ductility and decreased cracking tendency in the chromium-rich alloys were related to their increased strength, and the presence of a fine antiphase domain microstructure.

M. C. MAGUIRE is with Sandia National Laboratories, Process Metallurgy Div., Albuquerque, N.Mex. G. R. EDWARDS is with the Center for Welding and Joining Research, Department of Metallurgical and Materials Engineering, Golden, Colo. S. A. DAVID is with Materials Joining Group, Oak Ridge National Laboratory, Oak Ridge, Tenn.

Introduction

Polycrystalline Ni_3Al and alloys based on this intermetallic compound are of current interest due to their promising high temperature strength. Earlier problems with brittleness have been overcome, at least in part, by microalloying with boron (Refs. 1, 2) leading to further exploitation of the unusual dependence of strength on temperature. It has long been known that Ni_3Al possessed a positive temperature dependence of yield stress up to about 700°C (1292°F) (Ref. 3), hence, overcoming brittle fracture behavior in polycrystals made these alloys candidates for high-temperature structural applications. However, heat-affected zone (HAZ) cracking during welding and poor hot ductility showed that although boron was effective at promoting ductility in the low-temperature range of 25° to 500°C (77° to 932°F), other factors were limiting ductility at higher temperatures (Refs. 4–6). Utilizing monolithic Ni_3Al-type alloys as viable high-temperature materials cannot be fully realized until a better understanding of the factors that limit their weldability exists.

The first work on the weldability of boron-doped Ni_3Al alloys by David and coworkers (Ref. 7) showed that iron-containing alloys were susceptible to fusion zone and HAZ cracking during autogenous gas tungsten arc (GTA) welding. Subsequent work by Santella, *et al.* (Ref. 8), demonstrated that boron content affected cracking behavior. A boron concentration of 200 wppm produced the best cracking resistance. HAZ cracks were intergranular in nature with no evidence of liquation. The orientation of the HAZ cracks suggested that they formed during the welding operation and were the result of longitudinal welding stresses that occurred during the cooling portion of the weld thermal cycle. The cracking phenomenon in these alloys is generally attributed to intrinsically weak grain boundaries. However,

KEY WORDS

Weldability
Hot Ductility
Cr-Modified Alloys
Ni_3Al Alloys
Chromium Additions
Microstructure
Prior Heat Treatment
Oil-Quenched Alloys
Furnace-Cooled
SEM Fractography

Table 1 — Alloy Compositions Used in This Study, wt-% (at.-%)

Designation	Ni	Al	Cr	Hf	B
CR-2	85.5 (76.4)	10.8 (21.0)	1.98 (2.0)	1.70 (0.5)	0.02 (0.10)
CR-4	84.0 (75.4)	10.3 (20.0)	3.98 (4.0)	1.70 (0.5)	0.02 (0.10)
CR-6	82.7 (74.4)	9.70 (19.0)	5.91 (6.0)	1.67 (0.5)	0.02 (0.10)
CR-8	81.3 (73.4)	9.16 (18.0)	7.85 (8.0)	1.67 (0.5)	0.02 (0.10)

Santella, *et al.*, showed that crack-free welds could be made on some boron-doped Ni_3Al alloys with up to 10 at.-% iron (Ref. 9) and 0.5 at.-% hafnium (Ref. 10). Both elements were found to improve resistance to HAZ cracking; however, iron levels above 10 at.-% tended to promote formation of the β phase NiAl. There was no clear correlation between intergranular β formation and cracking tendency, although β is usually considered an unfavorable microconstituent due to its intrinsic brittleness. Autogenous GTA welds made on as-cast Ni_3Al with hafnium additions showed severe HAZ cracking owing to microsegregation of hafnium, aluminum and nickel in the original solidification structure (Ref. 10). As a result, although defect-free autogenous electron beam (EB) and GTA welds were made on wrought sheet and powder metallurgy compact, cast material with the same nominal composition experienced severe cracking during welding.

Despite promising results with welding studies on wrought material, hot ductility of these alloys is still generally low. Other investigators (Ref. 11) have recently demonstrated that HAZ cracking in Ni_3Al alloys cannot be solely attributed to poor hot ductility. Subsolidus HAZ cracking in materials with limited hot ductility results from the interaction between thermally generated stresses during welding and the flow properties of the HAZ. If the thermally induced transient stresses generated in the HAZ during welding exceed the fracture strength of a material, then one can expect cracking. Santella (Ref. 11) has shown that both poor hot ductility and sufficiently large thermal stresses are necessary for HAZ cracking of Ni_3Al alloys. It follows that increasing the hot ductility or strength would improve HAZ cracking resistance.

Recent studies by Liu and coworkers (Refs. 12, 13) have shown that Ni_3Al alloys are subject to embrittlement by environmental effects. This phenomenon, known as dynamic embrittlement, was first observed during hot tensile tests of Ni_3Al-based alloys. Liu observed that, over a certain temperature range, specimens tested in air failed with less plasticity than specimens tested in vacuum. Dynamic embrittlement may be contributing to the ductility loss of these alloys, but Santella (Ref. 11) showed that the embrittling effect does not appear to be a factor at temperatures over 800°C (1472°F) in hot ductility tests.

Adding chromium to Ni_3Al decreases the ordering transition temperature, T_t, thereby permitting formation of antiphase domains (referred to hereafter as APDs or domains) upon cooling of disordered γ (Ref. 14). When disordered γ is rapidly cooled, the random face centered cubic arrangement of atoms transforms to ordered γ by fine nucleation and growth of ordered APDs. Inoue showed that APDs formed in a number of Ni_3Al alloys with ternary transition metal additions when they were rapidly solidified by melt spinning (Ref. 16). In that study, alloys with chromium additions were ductile despite the absence of boron, and they suggested that the APDs were effective at hindering superlattice dislocation motion, thus preventing grain boundary loading by superlattice dislocation pileups. Huang and coworkers further confirmed the beneficial effects of APDs (Ref. 15) by showing that rapidly solidified Ni-Al-Cr ribbons without boron had substantial ductility at room temperature, and likewise concluded that the ductility was somehow linked to the APD microstructure.

The purpose of this work was to investigate the effect of APDs on the hot ductility and weldability of Ni_3Al alloys. As yet, little consideration has been given to whether or not APDs have any effect on hot ductility of Ni_3Al alloys. Additions of chromium coupled with heat treatments produced microstructural variations in four alloys. The microstructural features of each alloy in both conditions were characterized, and Gleeble testing on-heating determined quantitative differences in hot ductility in heat-treated samples. These results were then compared with EB welding behavior.

Materials and Experimental Details

Compositions of the four alloys chosen for this study are shown in Table 1. The chromium content for each alloy was chosen by evaluating an aluminum equivalent. Ternary solubility lobe behavior (Ref. 17) of the γ phase indicates that hafnium substitutes for aluminum in the ordered structure, while chromium substitutes equally on both sublattices. The aluminum equivalent, Al_{equiv}, was formulated as,

$$Al_{equiv} = \%Al + \%Hf + 0.5\%Cr = 22.5\% \text{ (at.-\%)}$$

Table 2 — Heat Treating Designations Used in This Study

Designation	Heat Treating Procedure
1190-FC	Anneal for 3.6 ks at 1190°C, furnace cool to 20°C(1)
1240-OQ	Anneal for 900 s at 1240°C, drop quench in oil at 20°C(2)
1270-OQ	Anneal for 900 s at 1270°C, drop quench in oil at 20°C(2)

(1) Vacuum anneal of 10^{-3} torr.
(2) Annealed in flowing argon.

An aluminum equivalent of 22.5% approaches the solubility limit of Ni_3Al (Ref. 17), indicating that stable disordered γ may be present at room temperature. Each alloy also contained boron and hafnium additions for reasons stated previously. All alloys were prepared by arc melting pure starting materials under an argon atmosphere. Boron levels were adjusted by proper addition of a 4 wt-% boron master alloy. Several remelts were used to ensure homogeneous mixing, followed by drop casting into chilled copper molds. The resulting 400-g (0.9-lb) ingots measured 9.5 X 25 X 127 mm (⅜ X 1 X 5 in.). Final chemical compositions were not verified, but based on significant experience with Ni_3Al alloy preparation by this process, alloy compositions do not vary significantly from nominal compositions. The ingots were homogenized at 1190°C (2174°F) in a vacuum of 10^{-3} torr or lower for 14.4 ks (4 h). Ingots were reduced in thickness by two cold forging steps, each reducing the thickness by 25% with intermediate 3.6 ks (1 h) anneals at 1190°C followed by furnace cooling. Hot ductility sample blanks were cut from these forged ingots for later heat treatment. However, owing to size limitations, samples for differential thermal analysis (DTA) to determine solidus and liquidus temperatures were cut from as-cast ingots. Based on DTA results, the maximum annealing temperature was determined. Although these temperatures were valid for as-cast material, the actual peak annealing temperatures used for study were slightly higher (10°C, 18°F) for the homogenized and worked material. Heat treatments used in this study are shown in Table 2. The 1190-

Table 3 — Experimental Welding Parameter Full Penetration Autogenous EB Welds

Welding Speed (mm/s)	Acc. Voltage (kV)	Beam Current (mA)	Heat Input (J/mm)
2.12	60	2.2	62.3
4.23	60	2.5	35.5
12.7	60	4.5	21.3
25.4	60	6.8–7.2	15.3–16.5

FC cycle was chosen to minimize APD structure, whereas the 1240-OQ cycle was designed to maximize APD formation. One alloy, CR-8, was also heat treated at 1270°C (2318°F) followed by an oil quench; this heat treatment was likewise designated 1270-OQ. No incipient melting was detected in any of the samples. After heat treating, the alloys were successively cold rolled 10 to 25% per pass with intermediate anneals at 1190°C for 3.6 ks (1 h) to reduce the thickness to 0.76 mm (0.03 in.).

Microstructures of the sample blanks were examined by light and transmission electron microscopy (TEM) to determine the extent of APD formation, and to characterize APD morphology. Thin foils for TEM were prepared by standard wafering and mechanical grinding techniques, followed by jet polishing in a perchloric acid electrolyte described elsewhere (Ref. 7). Foils were examined in a Phillips EM400 operating at 120 kV. Domain sizes were measured from TEM plates by linear intercept techniques, with no multiplication factors.

Hot ductility samples were prepared from the heat treated samples. Sample geometry is shown in Fig. 1. The hot duc-

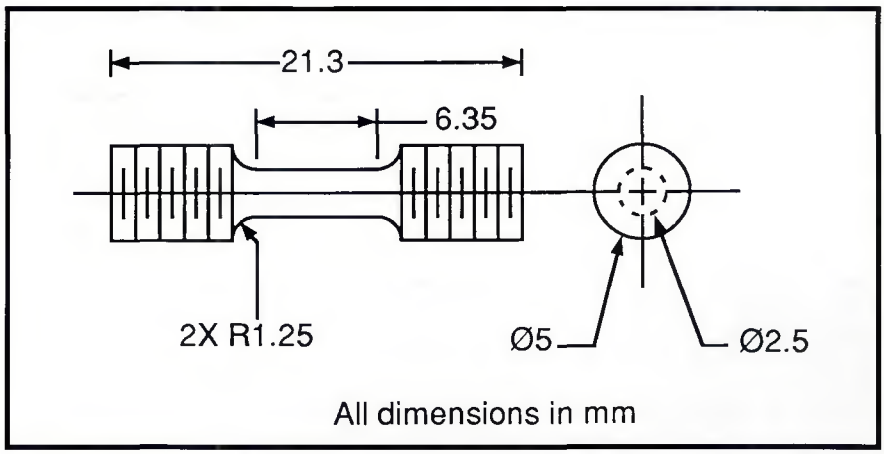

Fig. 1 — Hot ductility sample geometry used in Gleeble hot ductility test. Sample geometry and gripping assembly were optimized to produce shallow thermal gradients across the gauge length.

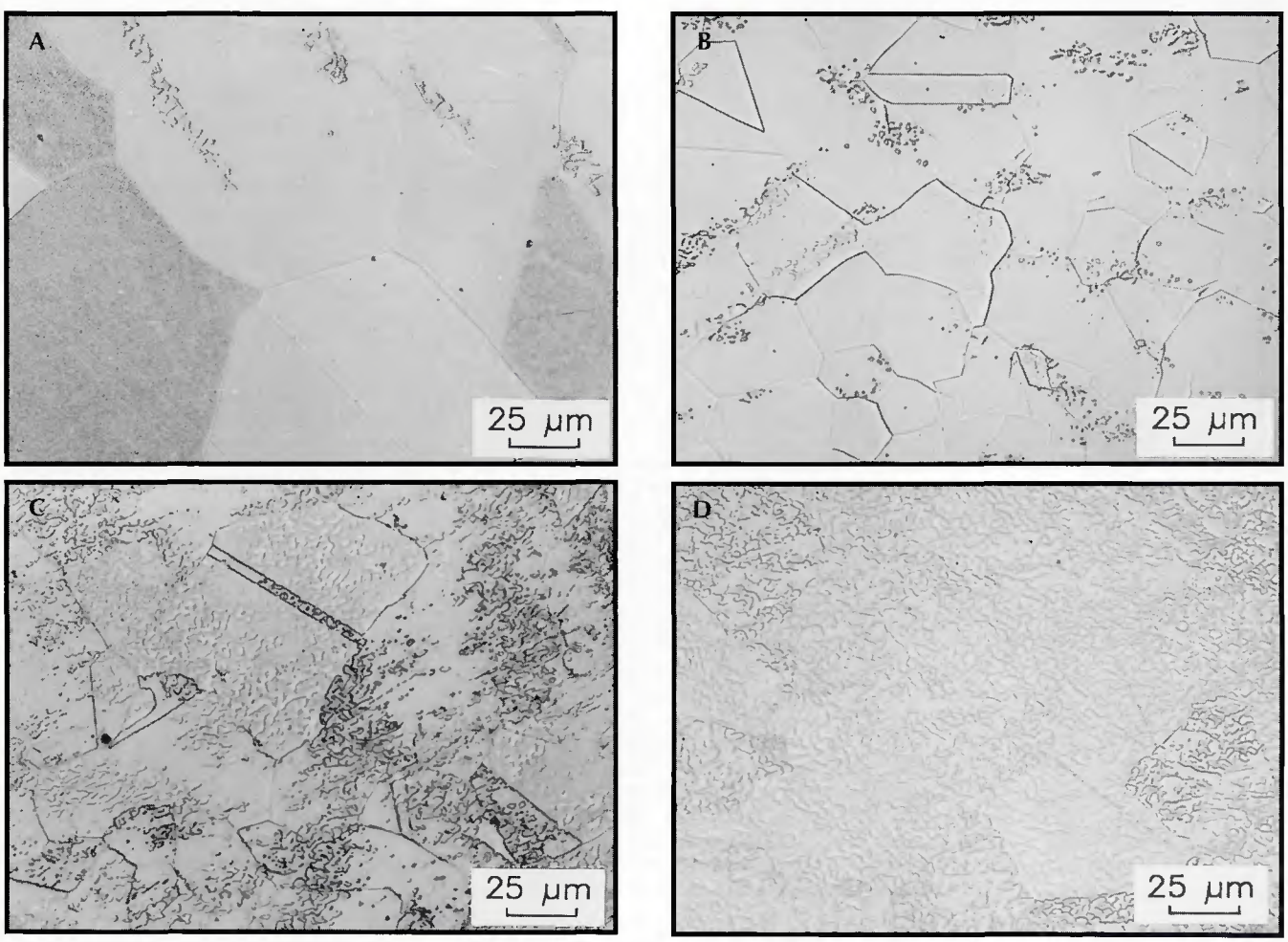

Fig. 2 — Light micrographs of the four chromium-containing alloys in the 1190-FC condition. A — CR-2, 2 at.-% chromium; B — CR-4, 4 at.-% chromium; C — CR-6, 6 at.-% chromium; D — CR-8, 8 at.-% chromium. (Etchant: saturated MoO_3 in 20% HF).

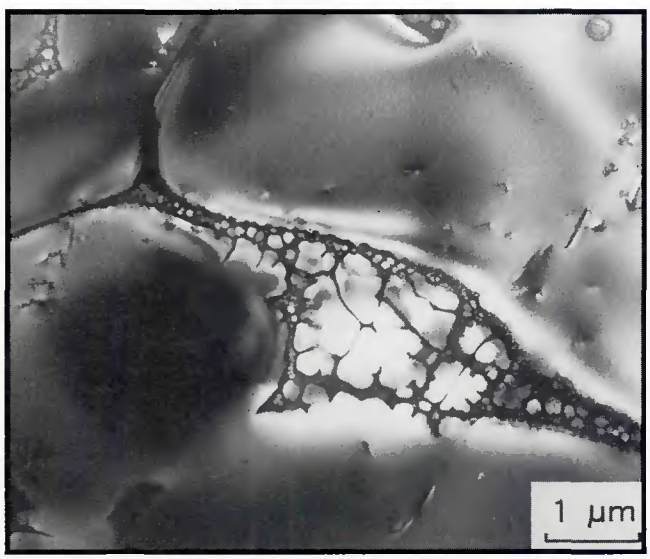

Fig. 3 — Centered dark-field transmission electron micrograph of CR-8 in the 1190-FC condition. Disordered γ forms a web-like network around ordered domains. The remaining matrix is ordered γ. Foil normal is near [110], g = 001.

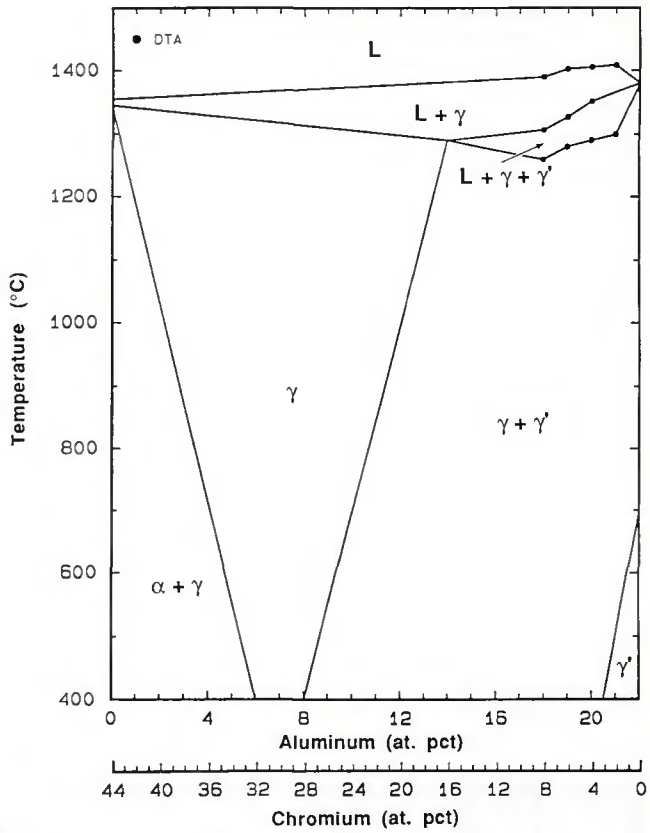

Fig. 4 — Estimated partial pseudobinary diagram for 22.5% Al_{equiv} alloys in this investigation. Liquidus and solidus temperatures were determined from DTA, whereas solid-state reactions are taken from the literature (Ref. 17).

tility test, described in detail elsewhere for Ni_3Al alloys (Ref. 8), subjects the sample to a simulated HAZ thermal cycle that is interrupted at various temperatures on-heating or on-cooling to fracture the sample. These tests were conducted in a Gleeble 1500 thermomechanical simulator equipped with digital data acquisition. Testing was performed only during the on-heating portion of the thermal cycle. Since one of the goals of this study was to determine the effect of APD hot ductility, reheating the sample above the peak temperature during the Gleeble thermal cycle would have significantly altered the initial microstructure. Testing on-heating with the rapid HAZ thermal cycle was used for minimizing structural changes in the heat treated samples. Specimens were fractured at a nominal strain rate of 0.1 s^{-1} and at temperatures from 25° to 1200°C (77° to 2192°F) during the heating portion of the thermal cycle. Ductility was measured as reduction in area at the fracture cross-section. Stress and strain data were acquired by a data acquisition system to determine yield stress and peak flow stress during the hot ductility test. Diametral strain was measured by a dilatometer mounted at the sample center. Fracture surfaces were analyzed by a JEOL JSM 840 scanning electron microscope (SEM), and fracture surface profiles were examined optically by sectioning the broken samples longitudinally. Samples for light microscopy were prepared by standard techniques throughout the investigation. Polished metallographic samples were etched in a saturated solution of MoO_3 in 20% HF.

Autogenous EB welds were made on 25 X 12 X 0.76-mm (1 X 0.5 X 0.03-in.) coupons. These coupons were prepared by successively cold rolling (10% reduction per pass) and annealing for 3.6 ks (1 h) at 1190°C followed by furnace cooling. Comparison of microstructures between the 1190-FC hot ductility samples (cold forged only) and the weld samples (cold forged + cold rolled) showed no detectable differences in grain size. In fact, grain size in the 1240-OQ or 1270-OQ samples also showed no detectable increase in size, the only exception being Alloy CR-2 where the grain size increased from 50 to 120 μm (mean linear intercept) in the 1240-OQ condition. The remaining alloys showed no differences in grain size between the hot ductility samples and the weld coupons. Welding was performed in a Leybold-Heraeus 1 5-kW electron beam welding machine with parameters adjusted to ensure full penetration. Experimental welding parameters are shown in Table 3. Weld coupons were loosely held in a copper jig that served to assure good electrical contact, but provided minimal constraint. Three samples were welded for each alloy. HAZ cracking frequency, measured as the number of cracks per mm of weld, was determined by visual observation of the weldments with a traveling microscope at 100X.

Results

Furnace-Cooled Microstructures

Light micrographs of the four alloys after the 1190-FC treatment are shown in Fig. 2. Alloy CR-2, which contains 2 at.-% chromium, is essentially single phase recrystallized γ (Ni_3Al), as seen in Fig. 2A. However, as the chromium content increases, a greater fraction of a second phase was observed. Selected area diffraction (SAD) analysis of TEM foils revealed the second phase to be disordered γ. Etching techniques tended to over emphasize the amount of γ in the microstructures shown in Figs. 2B, 2C, and 2D. Actual amounts of disordered γ were small, less than 5% in CR-8 when examined by TEM.

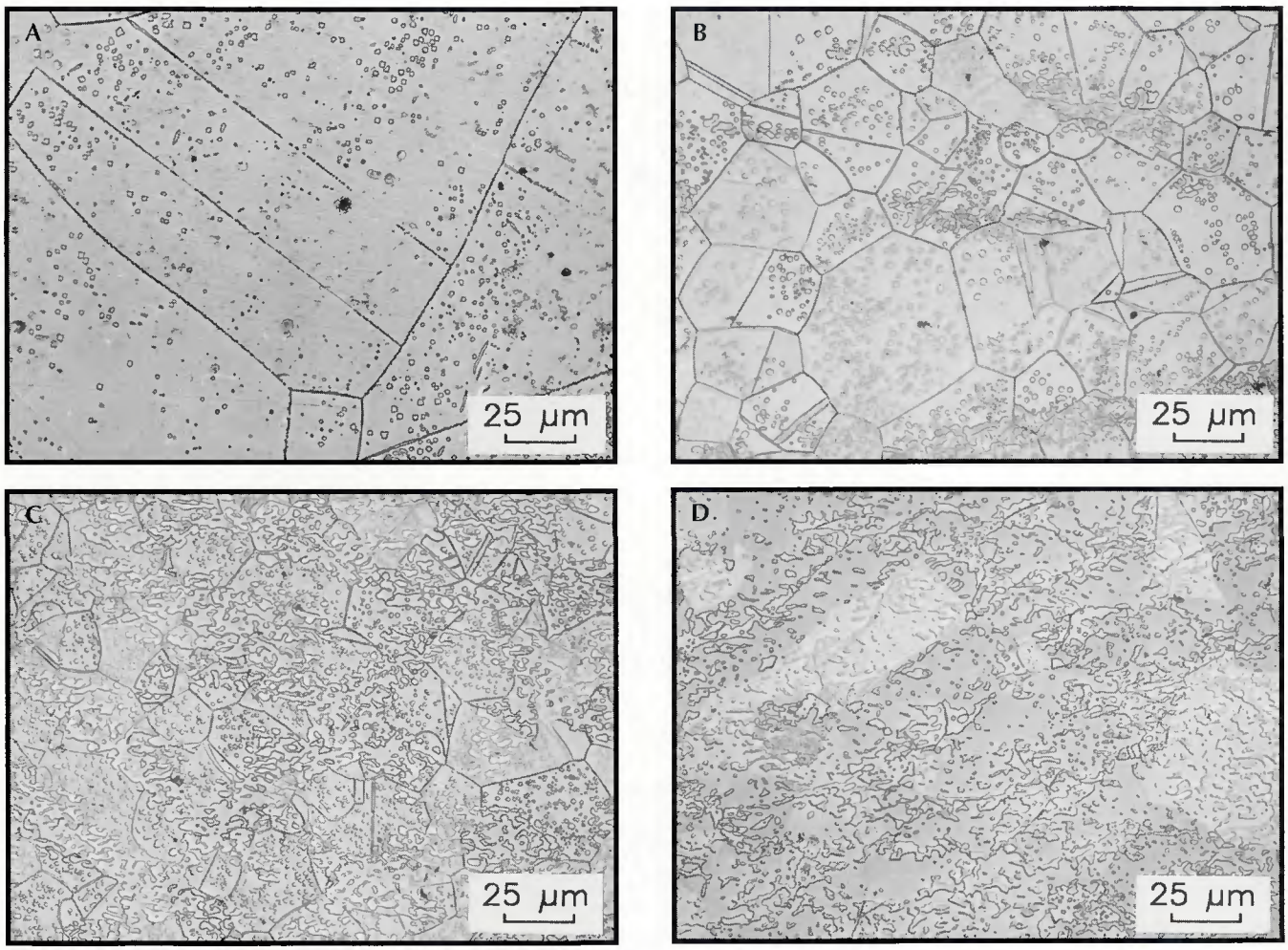

Fig. 5 — Light micrographs of chromium-containing Ni_3Al alloys after annealing at 1240°C for 900 s and oil quenching. A — CR-2, 2 at.-% chromium; B — CR-4, 4 at.-% chromium; C — CR-6, 6 at.-% chromium; D — CR-8, 8 at.-% chromium.

Figure 3 shows the appearance of the disordered second phase in CR-8. The disordered material surrounded cuboidal regions of the ordered matrix. Analysis of SAD patterns indicated that the disordered material had the same crystallographic orientation as the ordered matrix, consistent with observations of other investigators (Ref. 18). The localized regions of γ are most likely due to solute partitioning remaining from ingot solidification. Dendrite core regions would be lean in aluminum that would produce local regions of disordered γ. Metallographic observation of as-cast microstructures confirmed this morphology.

Quenched Microstructures

The amount of material that disorders during annealing at high temperature determines the maximum fraction of the microstructure that contains domains upon accelerated cooling. The ordering reaction in Ni_3Al is thermodynamically first order and cannot be suppressed in these alloys by quenching. Hence, cooling rate and composition determine the domain size, whereas composition alone determines the equilibrium fraction of disordered γ present at any temperature. Figure 4 shows the estimated isopleth of the Ni-Al-Cr system at an Al_{equiv} of 22.5 determined from DTA and from pertinent literature (Ref. 17). The effects of boron and hafnium were neglected for the construction of the isopleth. Liquidus and solidus temperatures were taken from the on-heating portion of the DTA thermogram, with the first deviation from the baseline interpreted as the solidus and the peak in the endotherm as the liquidus. Of the four alloys in this study, Alloy CR-8 experienced the greatest disordering prior to melting, but did not fully transform to γ, as confirmed by the microstructure shown in Fig. 5D. Microstructures of the other alloys after the 1240-OQ treatment are also shown in Fig. 5. The series of light micrographs shows a greater tendency to disorder at 1240°C (2264°F) as the chromium content is increased.

The disordered γ present at 1240°C re-orders to form fine domains if cooled at a sufficiently high rate. Small cuboidal regions are visible in Fig. 5A and indicate that a very small fraction of the microstructure disordered at 1240°C in CR-2, consistent with the trends in the isopleth of Fig. 4. The disordered material nucleated both at intragranular regions and twin or grain boundaries. Figure 5B shows that disordering continued to a greater extent in Alloy CR-4, in which the grain boundary films thickened, and the intragranular islands lost the cuboidal appearance. Alloys with higher chromium content showed more disordering, until the disordered material eventually became the dominant microconstituent — Fig. 5C and D. However, even at lower chromium levels, the disordered material formed as a grain boundary film; hence, it was the continuous phase.

The presence of APDs, characterized by TEM analysis, conclusively establishes that disordering occurred during annealing. As stated, the fraction of APD-containing microconstituent present after quenching relates directly to the amount of disordered γ present at the

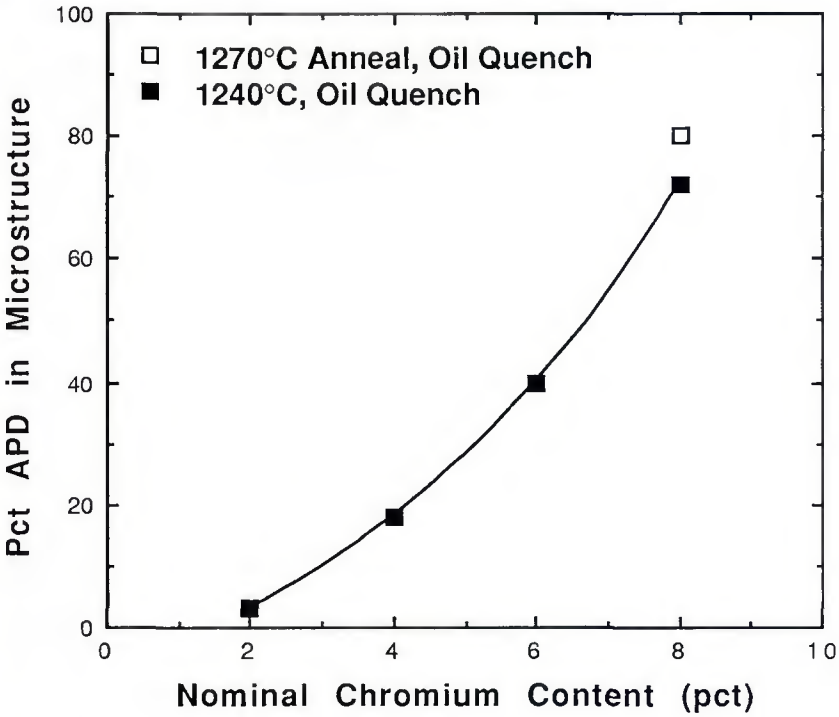

Fig. 6 — Effect of composition on the fraction of domain containing microconstituent in chromium-containing Ni_3Al alloys in the 1240-OQ condition.

annealing temperature. Figure 6 relates the chromium content to the fraction of APD-containing microconsitituent. As chromium content increased, the fraction of APD constituent increased, reaching 71% in CR-8 in the 1240-OQ condition. Domains were not observed in CR-2. The cuboidal regions seen in Fig. 5A could not be successfully imaged in TEM due to rapid coarsening and re-ordering under beam heating. It is suspected that these regions consisted of a few APDs. These domains were metastable at room temperature and rapidly disappeared leaving no residual contrast. APD microstructures are shown in Fig. 7 for CR-4, CR-6, and CR-8. The APD sizes for each of these alloys were 106, 53, and 44 nm, respectively. Imaging conditions were adjusted to "two beam" for a number of superlattice reflections. The antiphase boundaries (APB) did not disappear under any diffracting conditions, leading to the conclusion that the APBs contain a thin layer of disordered γ.

Hot Ductility Testing

The purpose of Gleeble testing for these alloys was to determine if the presence of a domain structure had any effect on hot ductility. APD structures can only be retained at room temperature by heating above the ordering transition temperature, and cooling sufficiently quickly to preclude their coarsening. Rather than rely on the HAZ thermal cycle simulation in the Gleeble to provide the APD structure for on-cooling tests, this study used heat treatments to produce well-characterized microstructures that were uniform along the length of the heated gauge section. Crack morphology in welds showed that nucleation sites lie in the HAZ just adjacent to the fusion line, consistent with areas that undergo disordering during the welding thermal cycle. An oil quench after annealing of the sample blanks was used to simulate the cooling experienced in the HAZ of the EB welds. Comparison of estimated cooling rates in the oil-quenched samples and calculated rates for actual welds are very similar at 300° and 200°C (572° and 392°F)/sec, respectively. Estimated cooling rates for welds were taken from a computational model described by Santella, *et al.* (Ref. 11), and quench rates were estimated from the work of Grossman and Bain (Ref. 19). These heat treated structures were tested on-heating to provide qualitative information related to the efficacy of APD structures at improving ductility.

Since ordering and disordering for Ni_3Al is extremely rapid, the HAZ immediately adjacent to the fusion line (the nucleation site for cracks) will disorder during heat-up and re-order just as with the oil-quenched samples during cooling. Hence, if an alloy shows differences in ductility related to the two heat treatments, one can infer its beneficial effect on HAZ cracking since the region of crack nucleation in welds will possess a similar microstructure.

On-heating hot ductility for the four alloys in the 1240-OQ condition is shown in Fig. 8. The major trends can be summarized as follows. Ductility decreases as the test temperature is increased, but the higher chromium alloys possess better hot ductility over the range of temperatures investigated. Previous investigations with a similar chromium-free alloy have shown that ductility at 600°C (1112°F) is very low, approaching zero (Ref. 20). Alloy CR-8 shows more than 15% reduction of area under these conditions.

When comparing the oil-quenched to slow-cooled microstructure, only Alloy CR-8 shows any effect of heat treatment on ductility. Figure 9 compares the hot ductility of Alloy CR-8 in two heat-treated conditions. The upper curve represents hot ductility in oil-quenched material, whereas, the lower curve represents furnace-cooled material. On-heating ductility is improved in the oil-quenched material at temperatures below 700°C. However, for the alloys with lower chromium contents, no difference in hot ductility behavior was observed between the slow-cooled and quenched microstructures. Although the ductility of these alloys improves as chromium content increases, no effect of heat treatment is apparent until a value of 8% chromium is reached.

In addition to the improved ductility encountered as chromium increased, flow stresses also increased. Figure 10 shows ultimate tensile stress (UTS) and yield stress data for the alloys at 20°, 600° and 1000°C (68°, 1112° and 1832°F). The UTS increased for each of the temperatures — Fig. 10A. Yield stresses, shown in Fig. 10B, were relatively constant between 20° and 600°C, but dropped substantially at 1000°C. Yield stress was relatively insensitive to alloy composition, whereas, the peak flow stress increased with higher chromium content, particularly so at room temperature.

Comparisons of the yield and fracture stress for the two different heat treatments for each of the alloys did not show any immediate differences. One would expect a material that undergoes a substantial refinement of microstructure, in this case substructural refinement, to also experience an increase in flow stress. This was not observed with these alloys. Figure 11 compares the flow stress of Alloy CR-8 at different temperatures for both the 1190-FC and the 1240-OQ conditions. There appears to be no change in flow or fracture strength between the two conditions, yet there is substantial difference in hot ductility.

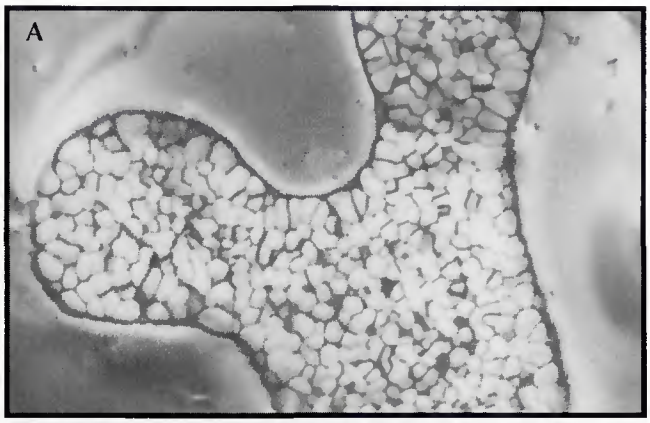

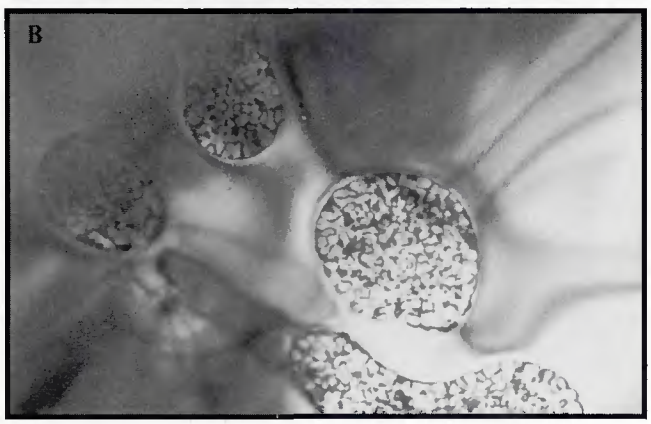

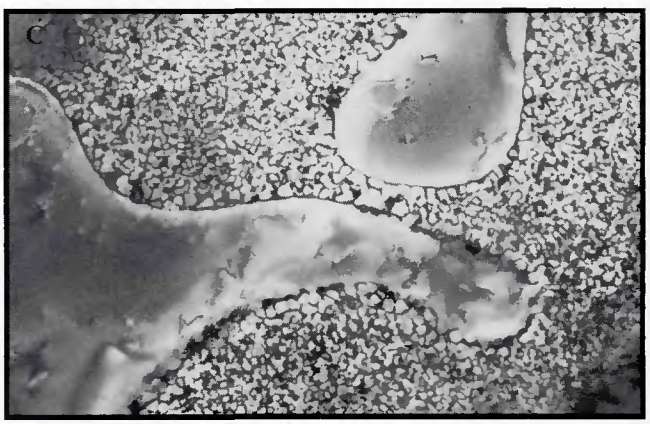

Fig. 7 — Centered dark-field transmission electron micrographs of domain microstructures in chromium-containing Ni_3Al alloys. The domain-containing regions are surrounded by the ordered $L1_2$ matrix. A — CR-4, 4 at.-% chromium; B — CR-6, 6 at.-% chromium; C — CR-8, 8 at.-% chromium. All imaging conditions used g = (001) with the foil normal near [110].

Fracture Appearance

SEM fractography was conducted on the fracture surfaces of the broken hot ductility bars. Figure 12 shows the fracture surface appearance of samples tested at 600°C for each of the alloys. Alloy CR-2, shown in Fig. 12A, showed completely intergranular fracture, while CR-4 and CR-6, shown in Fig. 12B and 12C, respectively, featured mixed mode fracture appearances, with small regions of transgranular fracture. However, the fracture was predominantly intergranular. Secondary cracks extending into the fracture surface were also observed in metallographic inspection of fracture profiles. In contrast, Alloy CR-8 displayed complete transgranular fracture behavior, with no observable intergranular decohesion, shown in Fig. 12D.

Electron Beam Welding

The cracking response of the four alloys as a function of chromium content is shown in Fig. 13. The cracking tendency decreased with increasing chromium at all welding speeds. As noted by other investigators, higher welding speeds aggravate the cracking phenomenon due to the greater stresses induced by thermal expansion and con-

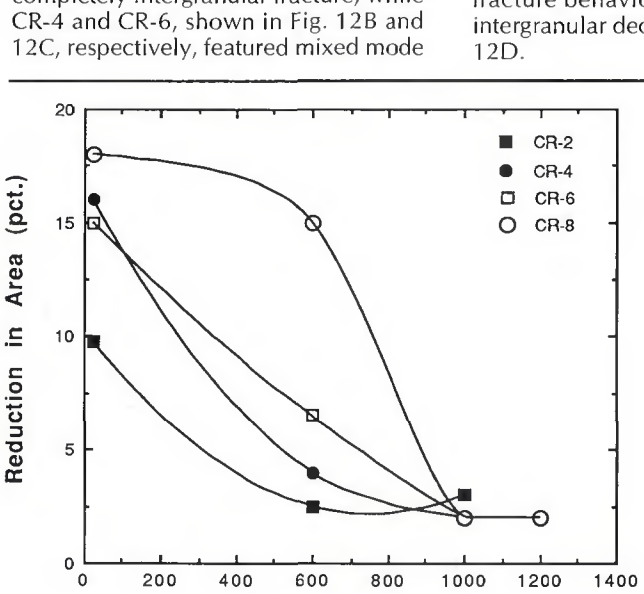

Fig. 8 — Reduction in area as measured in hot ductility testing of chromium-containing Ni_3Al as a function of temperature in the 1240-OQ condition.

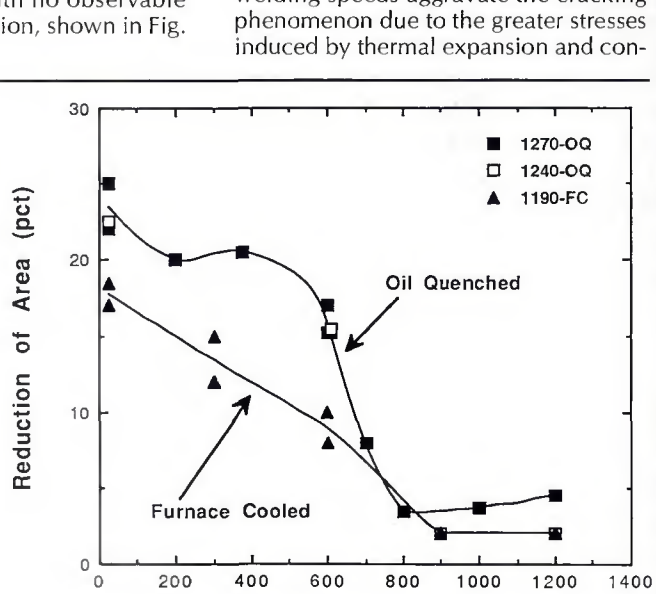

Fig. 9 —Hot ductility of Alloy CR-8 in the 1190-FC and 1240-OQ conditions as a function of temperature.

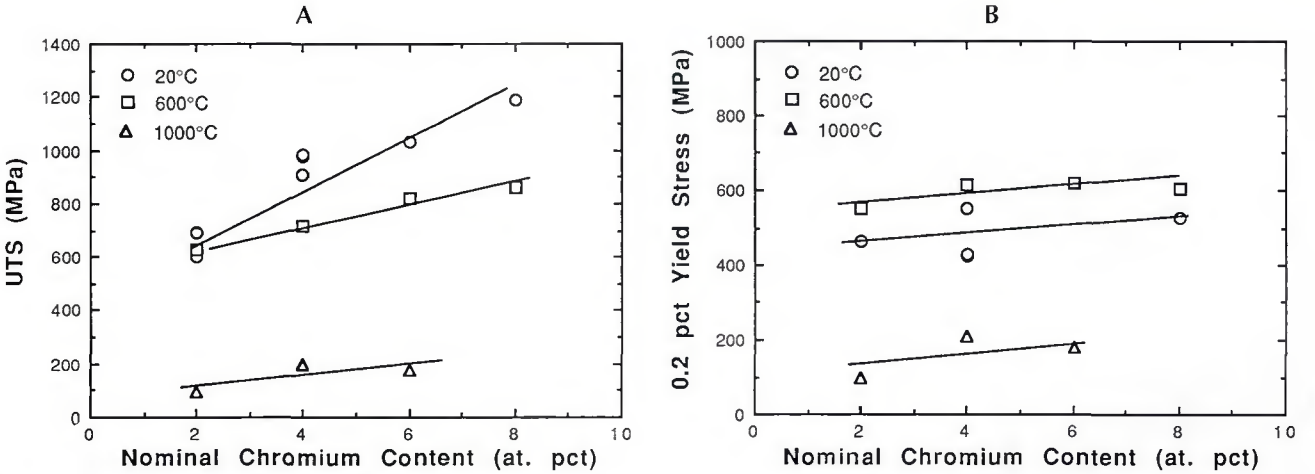

Fig. 10 — Strength data for hot ductility testing of chromium-containing Ni_3Al alloys as a function of temperature. A — Peak flow stress; B — 0.2% yield stress.

traction (Ref. 11). Cracks were primarily in the HAZ, although some did extend into the fusion zone. The cracks were found to have formed in the solid state and were not associated with any liquation phenomenon. Careful sectioning of welds to expose the crack surface followed by SEM analysis showed no evidence of a prior liquid phase in the HAZ cracks. In most cases a HAZ crack would also slightly extend into the fusion zone, shown in Fig. 13, but SEM analysis showed no evidence of liquated crack surfaces in these regions. Crack appearance is shown for Alloys CR-2, CR-4, and CR-6 in Fig. 14. Except for minor termination crater cracks at the highest welding speed, Alloy CR-8 did not crack.

Discussion

The tendency for improved weldability as chromium content increases is the primary finding of these experiments. Other investigators have correlated the weldability of Ni_3Al alloys with hot ductility and strength (Refs. 8, 9, 11). Low hot ductility has traditionally been considered to be the cause of HAZ cracking in these types of alloys. A more complete description of the cracking behavior observed in Ni_3Al was described by Santella, *et al.* (Ref. 11). Santella established that HAZ weld cracking can be avoided if the base metal has sufficient hot ductility, or if the welding stresses never exceed the fracture stress. Both of these characteristics are improved by chromium additions and APD substructures, and the proposed mechanisms are discussed below.

Intergranular fracture in polycrystalline Ni_3Al alloys is generally attributed to brittle grain boundaries, which fail prior to macroscopic plasticity (Ref. 21). However, this is not the only factor contributing to the ductility loss. Single crystals of Ni_3Al show the same ductility minimum with temperature (Refs. 22,23). The problem cannot solely be a grain boundary brittleness phenomenon. In addition, there is a strong dependence of hot ductility on grain size, for Ni_3Al alloys. In a separate study of another Ni_3Al alloy, other investigators found that grain sizes less than 20 μm were necessary to affect hot

Fig. 11 —0.2% offset yield strength for alloy CR-8 in the furnace-cooled and oil-quenched conditions.

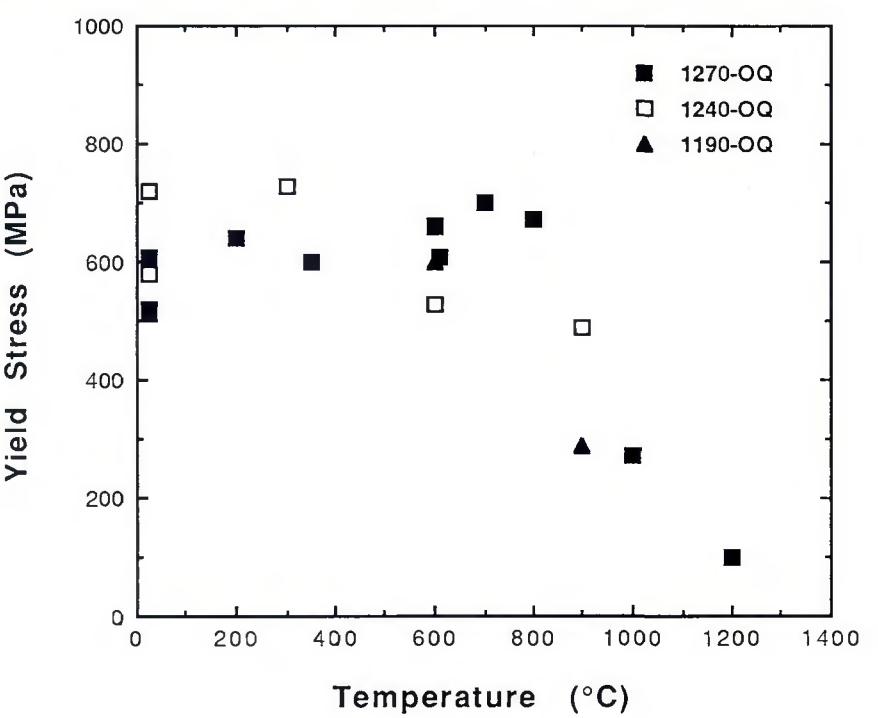

ductility at temperatures above 900°C (1652°F) (Ref. 20). Hence, microstructural refinement plays a role in improving hot ductility in Ni_3Al, presumably by refinement of the active slip path length. The possible mechanisms for such an influence follow.

Intergranular fracture in other materials is often the result of deformation constrained to a few selected slip planes. This localized deformation produces dislocation pileups at microstructural discontinuities, usually grain boundaries. These pileups increase the local stress on the grain boundary that nucleates intergranular cracking prior to slip in the adjacent grain. A well-known example of this occurs in deformation of ordered β-brass. This same mechanism is proposed to be operating in the Ni_3Al alloys.

Deformation at lower temperatures in Ni_3Al occurs primarily by motion of paired a/2[110]{111} dislocations that are bounded by a ribbon of antiphase boundary (APB). Pairwise motion is necessary to maintain the ordered structure in the wake of the dislocation. The unusual temperature dependence on flow stress is currently best understood by the cross-slip pinning (CSP) model (Ref. 24) that states that dislocations on the octahedral planes undergo thermally activated cross-slip to the [001] planes and become pinned. The frequency of the pinning mechanism increases with temperature and is driven by the lower antiphase boundary energy on the cube planes relative to the octahedral planes. As dislocations become pinned, the flow stress increases. In the absence of any APD substructure, the pinning mechanism is the primary influence on dislocation motion.

APD microstructures are not observed in binary stoichiometric Ni_3Al because no disordering occurs prior to melting (Ref. 14). However, by perturbing the stoichiometry or composition, the ordering transition temperature decreases to allow a fraction of disordered material to form. As shown by microstructures and phase equilibria, none of the alloys in this study could be fully disordered by heat treatment. The greatest amount of disordering, about 80% , occurred in Alloy CR-8 in the 1270-OQ condition. The hot ductility data shown in Fig. 9 indicates that this amount promotes increased hot ductility at temperatures less than 700°C. Ductility was not affected by heat treatment in any of the other alloys with less chromium. Despite a lack of improved hot ductility in these alloys, weld HAZ cracking decreased. This can be understood by considering the higher fracture stresses observed as chromium content increased. Using the data at 20°C from Fig. 10A, the fracture

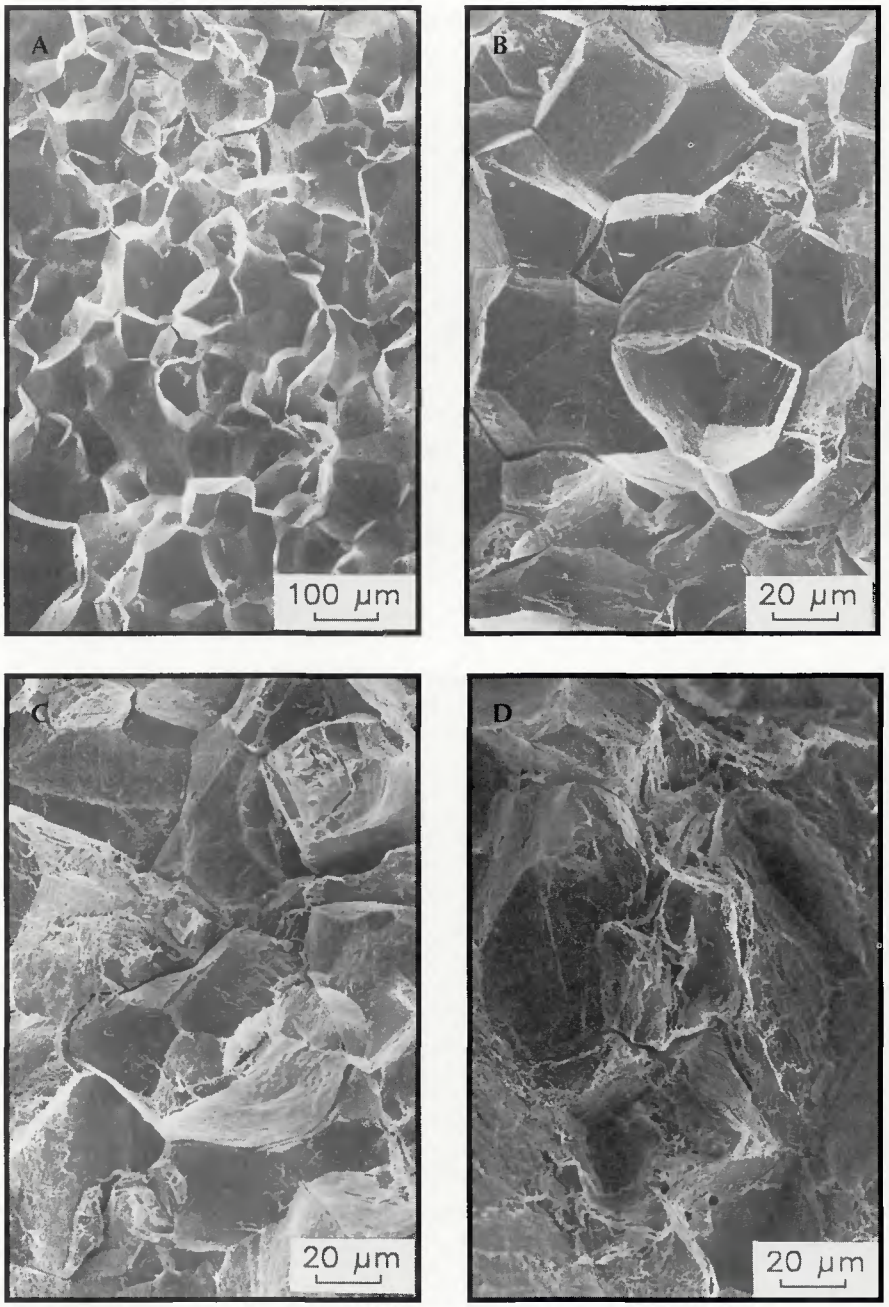

Fig. 12 — SEM fractographs of hot ductility samples fractured at 600°C. A — CR-2, 2 at.-% chromium; B — CR-4, 4 at.-% chromium; C — CR-6, 6 at.-% chromium D — CR-8, 8 at.-% chromium.

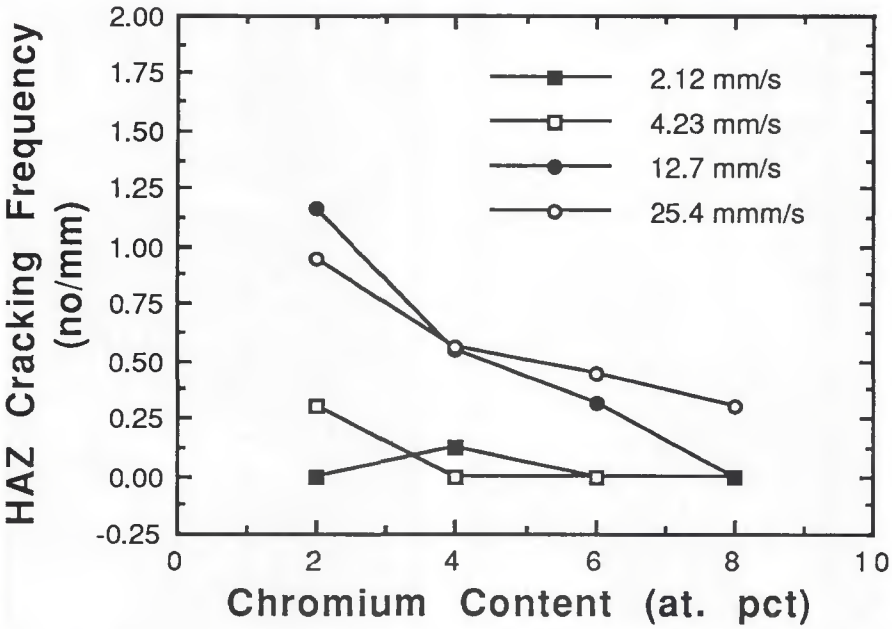

Fig. 13 — Cracking response of alloys during autogenous electron beam welding on 0.76 mm (0.030 in. sheet).

stress approximately doubles from 600 to 1200 MPa with an increase in chromium of 2 to 8 at.-%. The effect is not as potent at higher temperatures, but even at 600°C Alloy CR-8 is 30%, stronger than Alloy CR-2. This behavior is not dependent on heat treatment

As a result, it is not possible to determine the exact source of decreased cracking tendency in these alloys. Either the improved hot ductility, or the higher strength could be the source. If the source is strength, then its beneficial effect is apparent when considering the analysis by Santella (Ref. 11). Since Alloys CR-2, CR-4, and CR-6 showed no effect of heat treatment on ductility, their improved cracking resistance can only be attributed to the increase in flow stress. In Alloy CR-8, further increases in ductility were observed in APD microstructures representative of the HAZ. It is reasonable to expect that this improved ductility is also contributing to that alloy's cracking resistance. Although improved ductility clearly provides HAZ cracking resistance, the source of this improved ductility, particularly in Alloy CR-8 with the APD structure, is not as easily understood.

Two possible mechanisms, related to the presence of the APD microstructures, may be operating to cause the increase in hot ductility with high chromium content. The first is related to a decrease in the slip path length. In materials that deform by planar (coarse) slip, high local stresses can build up at the head of a dislocation pileup, usually at grain boundaries. An intergranular crack nucleates when the local stress at the tip of a pileup exceeds the cohesive strength of the boundary, producing grain boundary fracture. The number of dislocations present in the pileup after a given amount of deformation is directly related to a characteristic length of the slip path, most commonly the grain diameter. However, in some ordered systems, APDs are also effective barriers to slip. A simple analysis by Flinn (Ref. 3) yields,

$$t = \frac{2v}{a^2 d_{APD}\sqrt{3}}$$

where t is the shear stress necessary to cut an APB, v is the ordering energy, a is the usual lattice parameter, and d_{APD} is the APD diameter. Driving a dislocation through a domain boundary requires an additional energy input due to the creation of more APB. As a result, domain boundaries are barriers to dislocation motion, and effectively reduce the slip path length to the dimensions of the APD. Other researchers have shown this also to be true in other ordered systems, such as Ni_3V (Ref. 25). The presence of a large fraction of domains in the microstructure would then be effective at delaying the start of intergranular fracture by reducing the grain boundary loading by dislocation pileups. Although alloys with the same crystal structure as

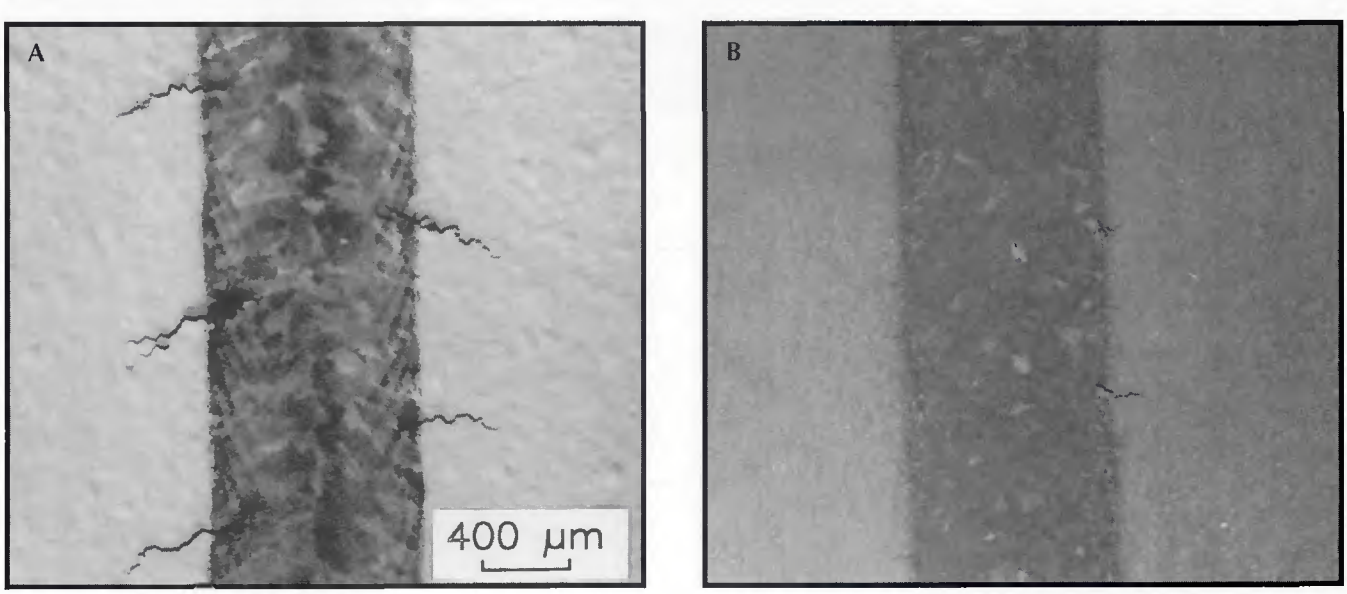

Fig. 14 — Light micrographs of electron beam welds in Ni_3Al alloys. A — Alloy CR-2; B — Alloy CR-4; C — Alloy CR-6; D — Alloy CR-8.

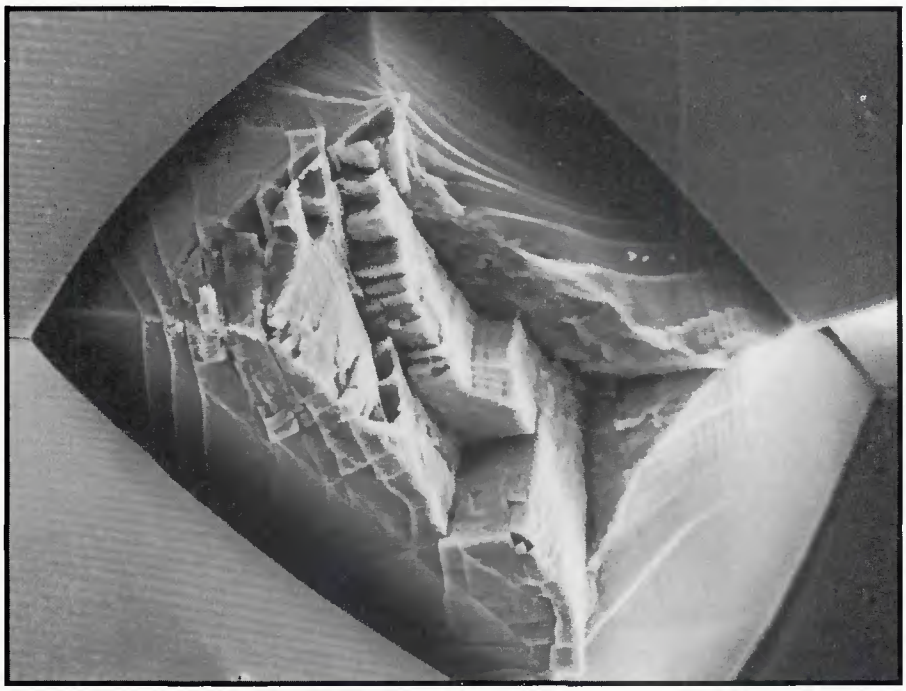

Fig. 15 — SEM fractograph of Alloy CR-2 fractured at 600°C showing slip offsets at grain boundary. Fracture was predominantly intergranular.

Ni_3Al, with high degree of order, are usually observed to deform by fine slip (Ref. 26), large slip steps on intergranular fracture surfaces are observed in the alloys in this investigation. Figure 15 shows a high-magnification SEM fractograph of a region of localized transgranular fracture in a hot ductility sample that fractured primarily by intergranular decohesion. The regions around the periphery are grain facets while the material in the center fractured in a transgranular fashion. Large slip steps are visible on the center grain, which has become detached from the surrounding grains, presumably due the process outlined above.

The second proposed mechanism for increased ductility is related to CSP model for strain hardening (Ref. 24). In this model, superlattice dislocations become immobilized by cross-slip pinning at certain points along the length of the dislocation. Further glide is then restricted without creation of new APB. Since cross-slip frequency is thermally activated, the average distance between cross-slipped segments on a dislocation line is constant for a given temperature, and in a simplistic argument, longer dislocations have more pinning points than shorter dislocations. By introducing an APD structure, not only would the slip path length decrease, so would the length of individual dislocations. It then follows that reducing the dislocation line length, or glide loop radius, allows for greater mobility of individual dislocations. In this event, strain hardening becomes less effective and the bulk stress should remain lower for a given amount of plastic strain. The result would then be increased ductility prior to failure. However, analysis of individual flow curves for oil-quenched and furnace-cooled samples of Alloy CR-8 show no difference in flow behavior.

Of the two mechanisms proposed, the first appears to be responsible for the increased ductility observed in the higher chromium alloys. It is interesting to note

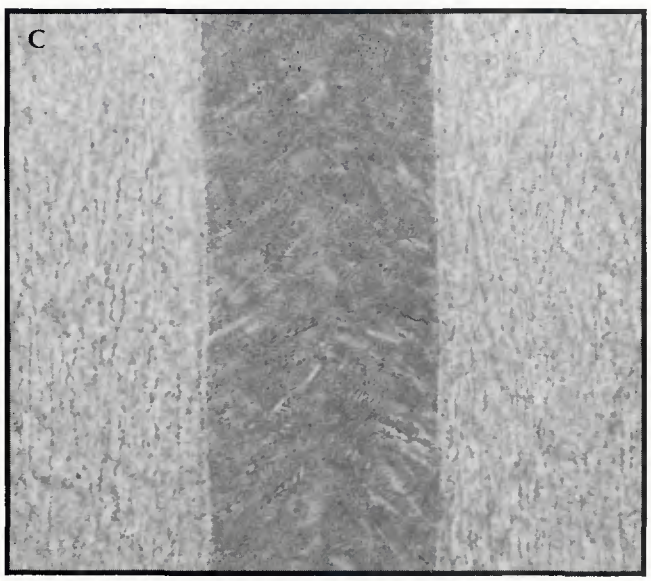

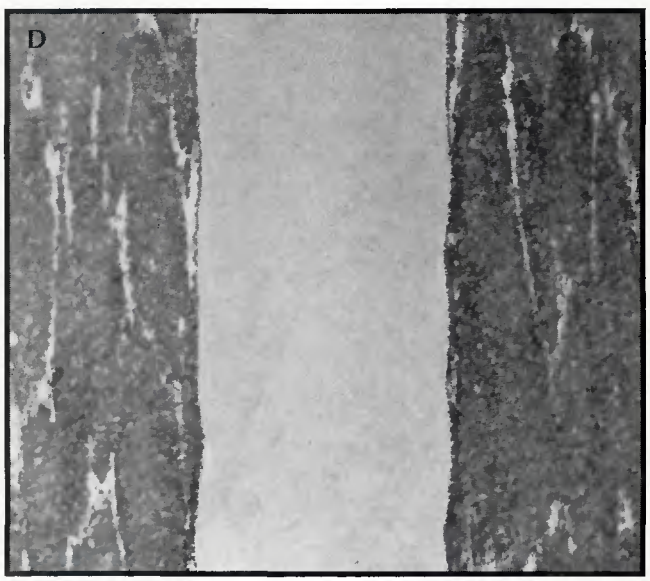

Welding speed equals 4.2 mm s^{-1}.

that although the ductility increased with the presence of the APD structure, flow stress appears unchanged. One would expect a refinement of slip path length to also increase the flow stress. The specific mechanism by which the APD structure affects dislocation motion is currently under consideration and will be the subject of a later publication.

Finally, Liu and coworkers (Refs. 12, 13) characterized the effects of dynamic embrittlement of certain Ni_3Al alloys at 600°C, and found that chromium appears to lessen the effect of atmospherically induced embrittlement. The present investigation shows that the effects of chromium can be extended to include microstructural effects and are not solely based on environmental mechanisms as proposed by Liu.

Conclusions

It is clear that weldability of Ni_3Al-based alloys is strongly dependent on a number of factors related to HAZ cracking susceptibility. From this work, two influences were characterized for an aluminum-lean base alloy: chromium content and prior heat treatment. Systematic additions of chromium that decreased the ordering transition temperature, when combined with heat treating, produced variations in microstructure. These variations were reflected in the relative amount of APD constituent present in the microstructure at room temperature.

Slowly cooled microstructures contained small regions of disordered γ surrounding coarse APDs in alloys containing more than 2 at.-% chromium. Alloy CR-2 (2 at.-% chromium) could not be disordered at 1240°C. Likewise, oil quenching produced APD structures in all alloys save CR-2. The fraction of the microstructure containing APD structure increased with chromium content of the alloys.

On-heating hot ductility was strongly dependent on chromium content, and to a lesser extent on prior heat treatment The alloy with 8 at.-% chromium (CR-8) exhibited noticeably more hot ductility in the oil-quenched condition relative to the slow-cooled condition. Alloys with lesser amounts of chromium did not show such behavior. This is likely attributed to the higher fraction of APD structure in Alloy CR-8, and its ability to reduce slip path length.

The welding response correlated well with strength and hot ductility. Higher chromium alloys showed improved resistance to intergranular cracking nucleated in the HAZ, and cracking was eliminated in an 8 at.-% chromium alloy. The cracking tendency increased with higher welding speed in alloys with less than 8 at.-% chromium.

Acknowledgments

The authors are grateful to C. V. Robino for reviewing the manuscript, R. W. Reed for technical assistance and V. K. Sikka for casting the alloys. This work was sponsored by the U.S. Department of Energy AR&TD Fossil Energy Materials Program DOE/FE AA 15 10 10 0, Work Breakdown Structure Element CSM-2, and by Sandia National Laboratories operated for the U.S. Department of Energy under contract DE-AC04-76DP00789.

References

1. Aoki, K., and Izumi, O. 1979. Nippon Kinzoku Gakkaishi 43:1190–1195.
2. Liu, C. T., and Stiegler, J. O. 1984. *Science* 226:636–642.
3. Flinn, P. A. 1960. Trans. TMS-AIME 218:145–154.
4. Aoki, K., and Izumi, O. 1978. *Trans. JIM.* 19:203–210.
5. Aoki, K., and Izumi, O. 1979. *J. Mater. Sci.* 14:1800–1806.
6. Maguire, M. C., Edwards, G. R., and David, S. A. *Scripia Met.* 22:1213–1217.
7. David, S. A., Jemian, W. A., Liu, C. T., and Horton, I. A. 1985. *Welding Journal* 64(1):22-s to 28-s.
8. Santella, M. L., and David, S. A. 1986. *Welding Journal* 65(5):129-s to 137-s.
9. Santella, M. L., David, S. A., and White, C. L. 1985. Proceedings of a Symposium on High-Temperature Ordered Intermetallic Alloys. Materials Research Society p. 496.
10. Santella, M. L., Horton, J. A., and David, S. A. 1988. *Welding Journal* 67(3):63-s to 69-s.
11. Santella, M. L., Maguire, M. C., and David, S. A. 1989. *Welding Journal* 68(1):19-s to 27-s.
12. Liu, C. T., and White, C. L. 1987. *Acta Met.* 35:643–649.
13. Liu, C. T., White, C. L., and Lee, E. H. 1985. *Scripta Met.* 19:1247–1248.
14. Cahn, R. W., Siemers, P. A., Geiger, I. E., and Bardhan, P. 1987. *Acta Met.* 35: 2737–2751.
15. Huang, S. C., Hall, E. L., Chang, K. M., and LaForce, R. P. 1986. *Met. Trans. A* 17A: 1685–1692.
16. Inoue, A., Masumoto, T., Tomioka, N., and Yano, N. 1985. *Int. J. Rapid Solidif.* 1: 115–142.
17. Merchant, S. M., and Notis, M. R. 1984. *Mat. Sci. Eng.* 66:46–60.
18. Horton, J. A., and Liu, C. T. 1985. Acta Met. 33:2191–2195.
19. Grossman, M. A., and Bain, E. C. 1964. *Principles of Heat Treatment,* 5th ed., ASM International, Materials Park, Ohio.
20. Edwards, G. R., Maguire, M. C., and Damkroger, B. K. 1989. Proceedings of the 2nd International Conference on Trends in Welding Research, ASM International, Materials Park, Ohio.
21. Takasugi, T., and Izumi, O. 1985. *Acta Met.* 33:1247–1258.
22. Copley, S. M., and Kear, B. H. 1967. *Trans. TMS-AIME* 239:977–984.
23. Takeuchi, S., and Kuramoto, E. Acta Met. 21:415–425.
24. Taoka, T. K., Yasukochi, K., and Honda, R. 1960. *The Mechanical Properties of Intermetallic Compounds.* Symposium of the 115th Meeting of the Electrochemical Society, Ed. J .H. Westbrook, John Wiley & Sons, New York.
25. Vanderschaeve, G., Sarrazln, T., and Escaig, B. 1979. *Acta Met.* 27:1251–1260.
26. Kear, B. H. 1966. *Acta Met.* 14:659–677.